Electronic Supplementary Information

Enhanced CO_2 electroreduction performance over Cl-modified metal catalysts

Huai Qin Fu,[a] Le Zhang,[a] Li Rong Zheng,[c] Peng Fei Liu,[*a] Huijun Zhao[b] and Hua Gui Yang[*a]

[a]Key Laboratory for Ultrafine Materials of Ministry of Education, School of Materials Science and Engineering, East China University of Science and Technology, Shanghai 200237, China.

[b]Centre for Clean Environment and Energy, Gold Coast Campus, Griffith University, Queensland 4222, Australia.

[c]Beijing Synchrotron Radiation Facility, Institute of High Energy Physics, Chinese Academy of Sciences, Beijing 100049, China.

[*] Corresponding author: hgyang@ecust.edu.cn; lpfxj1114@163.com.

Experimental Section

Chemicals. Silver nitrate ($AgNO_3$, 99.8%) and Lead foil (Pb) were purchased from Aladdin. Sodium chloride (NaCl, 99.5%), Polyvinyl pyrrolidone (PVP K-30), glycerol ($C_3H_8O_3$, 99%), Isopropanol (C_3H_8O, 99.7%), Sodium Borohydride ($NaBH_4$, 98%), and sodium citrate ($C_6H_5Na_3O_7$, 99%) were obtained from Shanghai Lingfeng Chemical Reagent. Lead Nitrate ($Pb(NO_3)_2$, 99%) was purchased from Sinopharm Reagent. Nafion (5 wt %) was purchased from Sigma-Aldrich. Carbon paper (TGP-H-060) and Nafion 115 proton exchange membrane were purchased from Alfa Aesar. The carbon fiber paper was ultrasonic with deionized water and ethanol for 30 min in sequence, then was treated with concentrated HNO_3 at 100 °C for 12 h, finally washed with water and ethanol many times and dried in air, to ensure that the surface of the carbon fiber paper was well cleaned before use.

Synthesis of AgCl nanoparticles. For the preparation of AgCl precatalysts, $AgNO_3$ (0.158 g) and PVP (0.586 g) were added into $C_3H_8O_3$ (19 mL) with continuous stirring (solution A). NaCl (0.059 g) was added into the solution mixed with $C_3H_8O_3$ (10 mL) and deionized water (0.5 mL) (solution B). Then the solution B was poured into solution A for stirring of 30 min. Finally the mixture was transferred into a 50 mL Teflon-lined stainless steel autoclave and kept at 160 ºC for 2.5 h. After the autoclave was cooled down to room temperature, the mixture was washed with ultrapure water and ethanol for several times and then dried at 60 ºC for 6 h in vacuum oven.

Synthesis of Ag nanoparticles. To synthesize Ag NP, $AgNO_3$ (0.5 g) was added into the deionized water (50 mL) (solution A). $C_6H_5Na_3O_7$ (0.25 g) was added into the deionized water (50 mL) (solution B), then mixing solution A with B for continuous stirring of 30 min (solution C). Afterwards, $NaBH_4$ (0.5 g) was dissolved into deionized water (25 mL) (solution D), then the solution D was quickly poured into solution C, subsequently stirring for 2 h. Finally, the mixture was washed with ultrapure water and ethanol for several times and dried at 60 ºC for 6 h in vacuum oven.

Synthesis of Pb(OH)Cl. To synthesize Pb(OH)Cl, 6.624 g $Pb(NO_3)_2$ and 1.1688 g NaCl were dissolved into 80 mL H_2O, and stirring for 0.5 h. Subsequently, 5 mL $NH_3 \cdot H_2O$ was added dropwise to deposit Pb^{2+} completely. The as-obtained white product was filtered and washed by distilled water several times, then dried in vacuum oven at 100 °C for 24 h.

Preparation of working electrodes. 10 mg AgCl nanoparticle, and 40 μL Nafion solution (5 wt%) were dispersed 500 μL isopropanol by 40 min sonication to form an ink solution. Then 50 μL of the resulting catalyst ink was drop-dried onto the carbon fiber paper substrate and another 50 μL was loaded onto the other side of carbon fiber paper to ensure full coverage of the substrate (1×1 cm^2).

Electrochemical measurements. The electrolyte (0.5 M $KHCO_3$; Sinopharm) was saturated with high-purity CO_2 (99.9999%) gas for at least 30 min to get a solution with pH of 7.2. Electrochemical measurements were performed in a two-compartment electrochemical cell and Nafion 115, as a proton exchange membrane, was used to separate the two sides. During CO_2 electrolysis, the electrolyte in the cathodic compartment was stirred at a rate of 800 r.p.m, and the flow rate of CO_2 was maintained at 5 sccm, which was measured by a universal flow meter (Alicat Scientific, LK2) at the entrance of the electrochemical cell. All the CO_2RR electrochemical tests were conducted in a conventional three-electrode system at an electrochemical station (CHI 660E), using as-prepared AgCl catalysts on carbon fiber paper as the working electrode, Ag/AgCl (3.5 M KCl solution) as the reference, and Pt mesh electrode as counter electrode, respectively. The CO_2 reduction reaction were measured by using chronoamperometric method under potential region from -0.4 to -1.2 V vs. RHE. All potentials were referenced to reversible hydrogen electrode (RHE) by following calculations: $E_{RHE} = E_{Ag/AgCl} + 0.059 \times pH + 0.205$. LSV curves were conducted at the scan rate of 5 mV s^{-1}. AC impedance measurements were carried out in the same configuration when the working electrode was biased at the potential of -0.65 V vs. RHE from 10^5 Hz to 0.01 Hz with an AC voltage of 5 mV. The chronoamperometric (E = -0.75 V vs. RHE) was conducted to evaluate the long-term stability. The gas chromatography (GC) system (RAMIN, GC2060) equipped with a flame ionization detector (FID) and a thermal conductivity detector (TCD) was used to detect and quantify the H_2 and CO, respectively. The volume fractions of evolved CO and H_2 from cathodic reduction were measured by gas chromatography after 30 min of electrolysis at each potential. The CO and H_2 Faradaic efficiency were calculated as below:

$$FE_{CO} = \frac{2x_{CO}pGF}{IRT} \qquad FE_{H_2} = \frac{2x_{H_2}pGF}{IRT}$$

Where x_{CO} and x_{H_2} (vol%) is the volume fractions of CO and H_2 in the exhaust gas, I (A) is the steady-state total current, G = 5 mL min^{-1} is the CO_2 flow rate, $p = 1.013 \times 10^5$ Pa, T = 273.15 K, F = 96485 C mol^{-1}, R = 8.3145 J mol^{-1} K^{-1}.

Electrochemically active surface area (ECSA) calculation. The ECSA was determined by lead (Pb) underpotential deposition (UPD) in a mixed solution containing 5.0 mM Pb(acetate)$_2$, 10.0 mM $HClO_4$, and 10.0 M KCl. Then the result was recorded by cyclic voltammetry at the potentials between 0.9 and -0.8 V vs. Ag/AgCl with the scan rate of 10 mV s^{-1}. The corresponding charge is 600 μC cm_{ec}^{-2} for Ag-based samples.[1]

Characterizations. The morphologies and structures of the samples were characterized by scanning electron microscopy (SEM, Hitachi S4800) and transmission electron microscopy (TEM, JEM-2100, 200 kV). The crystal structure was determined by X-ray diffraction (XRD, D/max2550V). The content of chloride ions was detected by ion chromatograph (IC, ICS-1100) Furthermore, the chemical states of the elements in catalysts were studied by X-ray photoelectron spectroscopy (XPS, Thermo Escalab 250), and the binding energy of C 1s peak at 284.8 eV was taken as an internal standard. Cl K-edge X-ray absorption structure (XAS) measurements were performed at the beamline 1W1B in Beijing Synchrotron Radiation Facility, China.

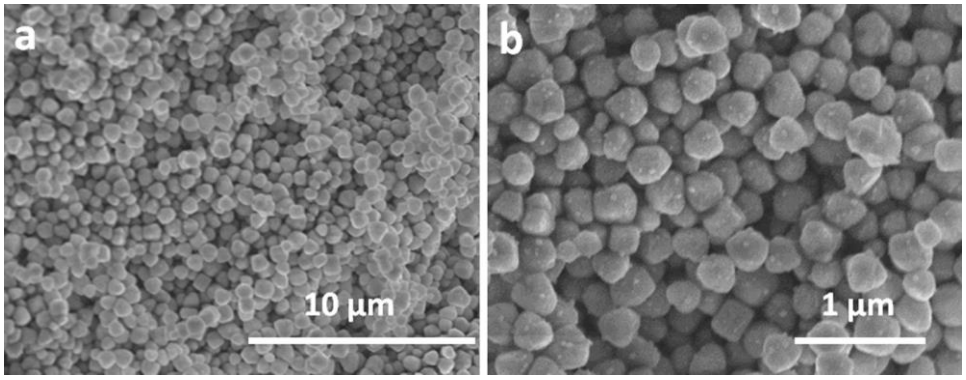

Fig. S1. (a, b) FESEM images of the pristine AgCl sample at different magnifications.

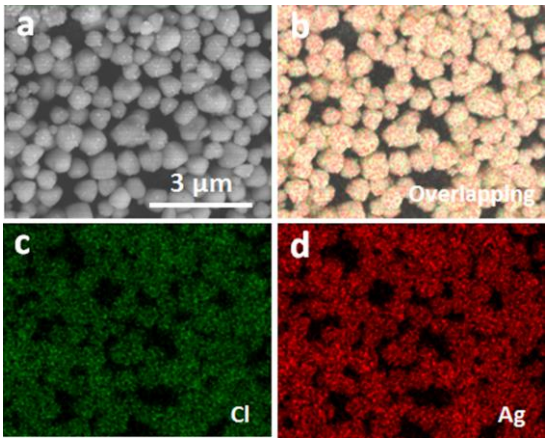

Fig. S2. (a) FESEM image of the pristine AgCl sample and corresponding elemental mapping images of (b) overlapping, (c) Cl, and (d) Ag.

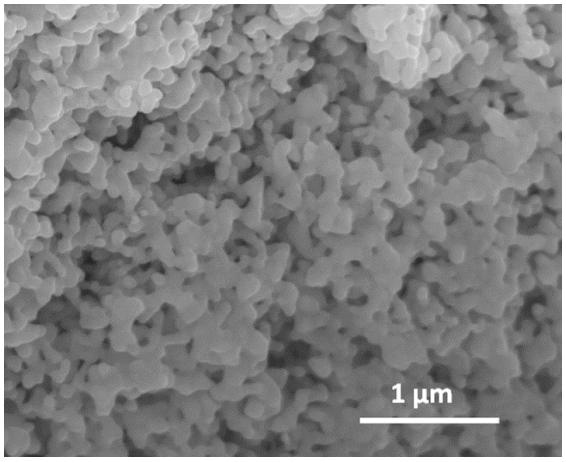

Fig. S3. FESEM image of the Ag NP reference sample.

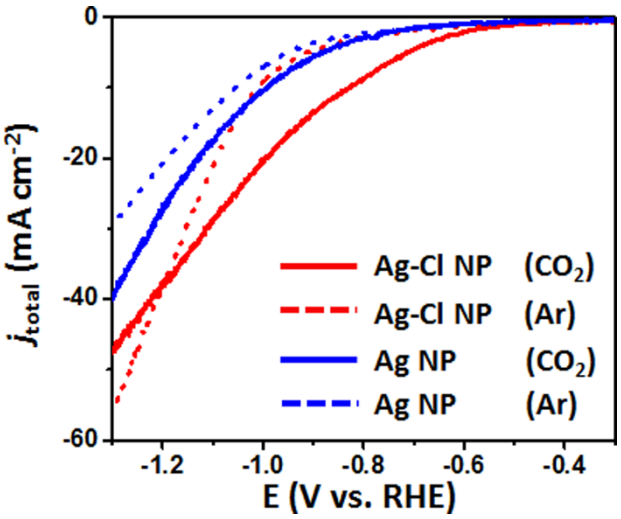

Fig. S4. LSV curves of Ag-Cl NP and Ag NP catalysts at different potentials ranging from -0.3 to -1.3 V vs. RHE. The polarization curves were obtained at the scan rate of 5 mV s^{-1} in CO_2-saturated and Ar-saturated 0.5 M $KHCO_3$ electrolytes, respectively.

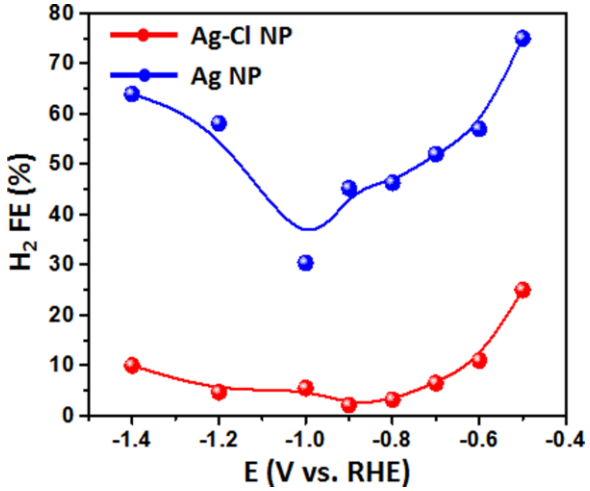

Fig. S5. H_2 Faradaic efficiency for Ag-Cl NP and Ag NP catalysts at different potentials ranging from -0.5 to -1.4 V vs. RHE. The Ag-Cl NP catalyst shows lower H_2 Faradaic efficiency, with below 10% under a wide potential region from -0.6 to -1.3 V vs. RHE.

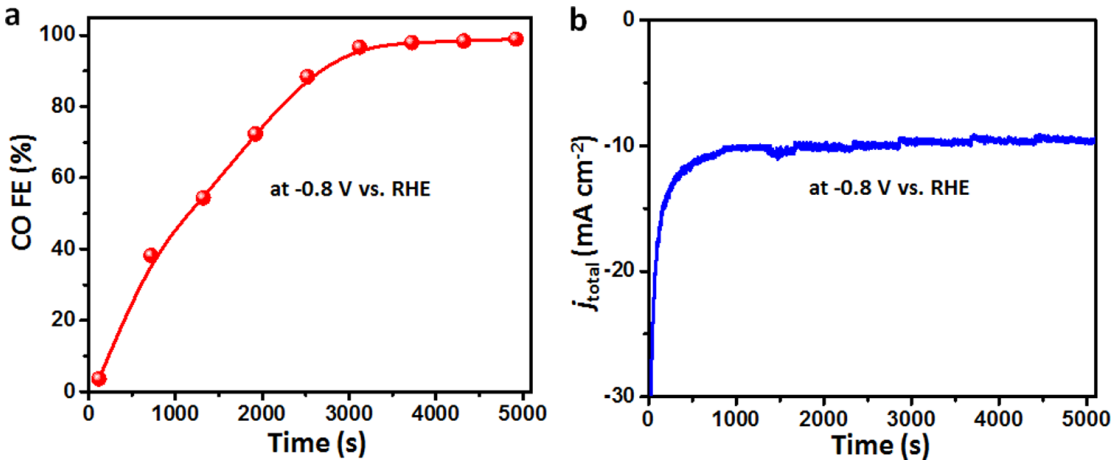

Fig. S6. (a) CO Faradaic efficiency and (b) total current density depending on time for pristine AgCl sample during the first 5000 s at the potential of -0.8 V vs. RHE.

Notes: The value of FE_{CO} becomes greater over time during the first 3000 s, while it keeps over 95% after electrolysis for 1 h. This part of the non-Faradaic current may be related to the reduction of Ag^{+}. This result clarifies that the Ag-Cl NP prepared via *in-situ* reducing AgCl precatalyst under CO_2 reduction conditions for about 1 h exhibits more excellent CO_2RR performance than pristine AgCl.

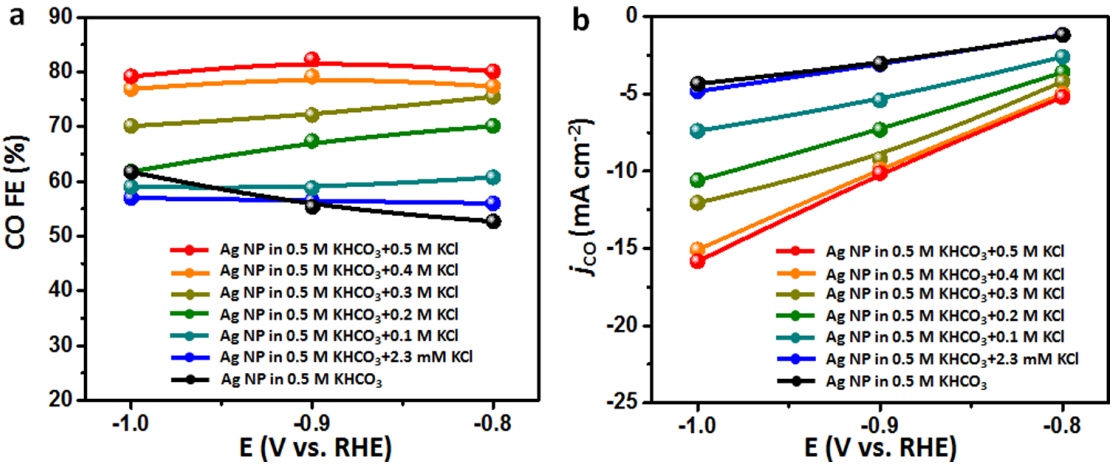

Fig. S7. (a) CO Faradaic efficiency and (b) CO partial current density of Ag NP catalysts tested in the different electrolytes (CO_2-saturated 0.5 M $KHCO_3$, mixed solution of 0.5 M $KHCO_3$ and 2.3 mM, 0.1 M, 0.2 M, 0.3 M, 0.4 M, and 0.5 M KCl).

Notes: The Ag NP exhibits greater FE_{CO} and j_{CO} with the increased concentration of Cl^- ions in the electrolyte, while the difference between the one in 0.4 M KCl and the one in 0.5 M KCl is small. This result reveals the influence of Cl^- ions in the electrolyte on the performance of CO_2RR, along with indicating that the 0.4 M KCl may reach the state of surface saturation for Ag NP in our catalytic system to some extent.

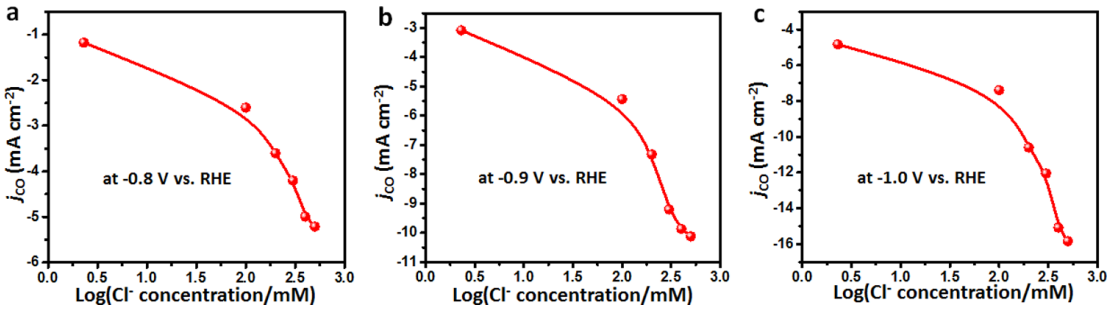

Fig. S8. CO current density depending on Log(Cl^- concentration) for Ag NP catalyst at the potentials of (a) -0.8, (b) -0.9, and (c) -1.0 V vs. RHE.

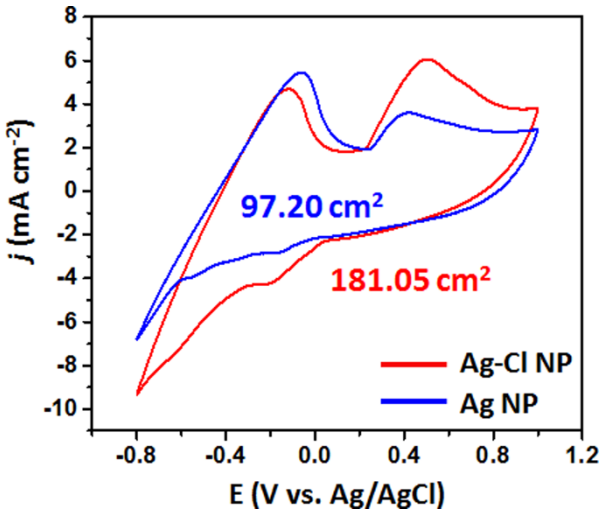

Fig. S9. Cyclic voltammograms of UPD and bulk deposition of Pb in a mixture solution containing 5.0 mM Pb(acetate)$_2$, 10.0 mM $HClO_4$, and 10.0 M KCl for overlap of Ag-Cl NP and Ag NP.

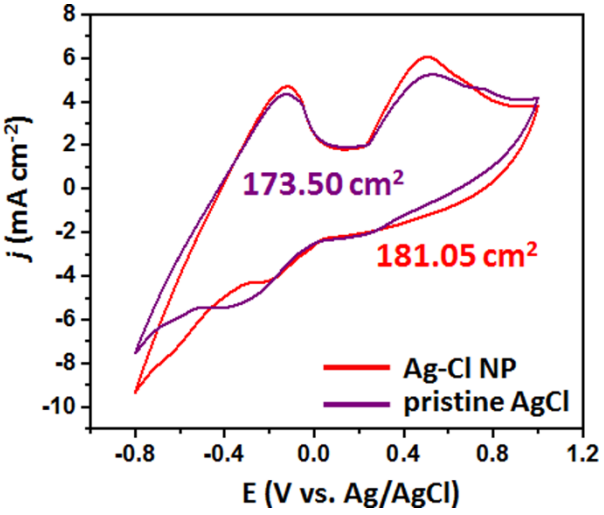

Fig. S10. Cyclic voltammograms of UPD and bulk deposition of Pb in a mixture solution containing 5.0 mM Pb(acetate)$_2$, 10.0 mM $HClO_4$, and 10.0 M KCl for overlap of Ag-Cl NP and pristine AgCl.

Notes: The ECSA of Ag-Cl NP is calculated to be 181.05 cm^2, and the ECSA of 173.5 cm^2 for pristine AgCl is close to the value of Ag-Cl NP, illustrating that the variation of surface active areas are negligible before and after reaction.

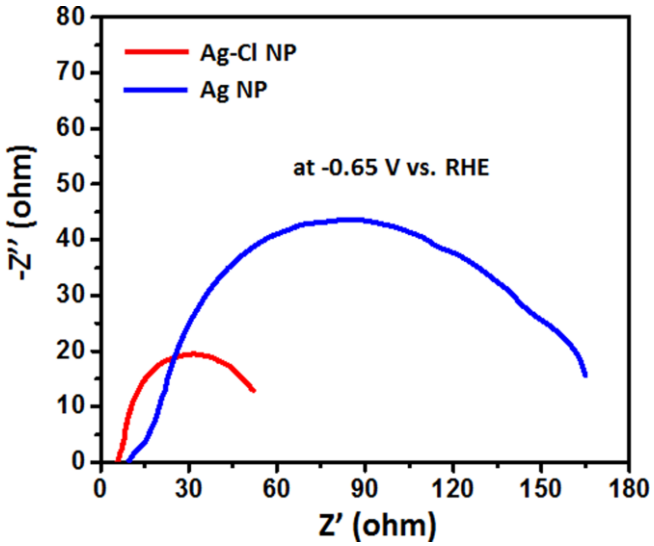

Fig. S11. The Nyquist plots of Ag-Cl NP and controlled Ag NP samples at the potential of -0.65 V vs. RHE.

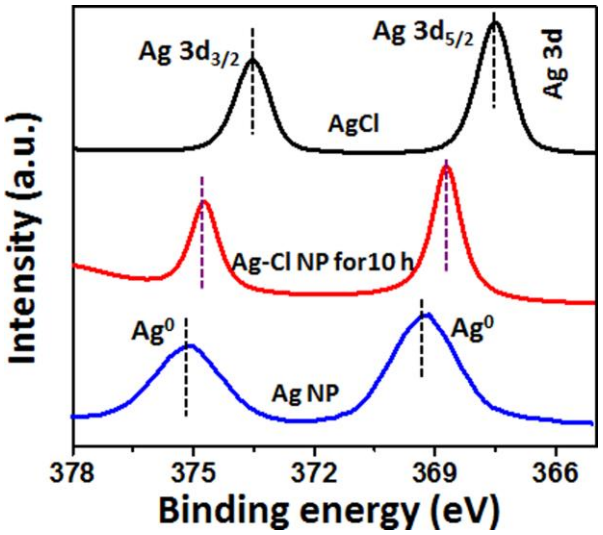

Fig. S12. The high-resolution XPS spectra for pristine AgCl, Ag NP, and Ag-Cl NP samples after 10 h potentiostatic measurement in the region of Ag 3d.

Notes: The peaks of 368.8 and 374.8 eV for Ag-Cl NP indicate that metallic Ag has formed, simultaneously a trace amount of Ag^+ is still retained on the surface during CO_2RR.

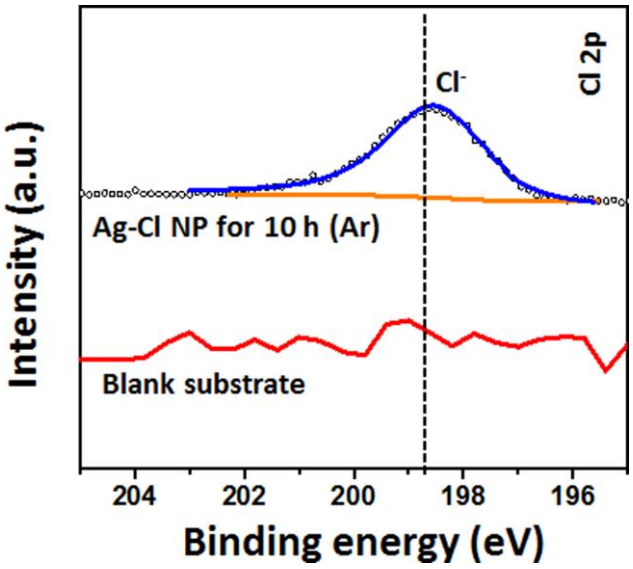

Fig. S13. The high-resolution XPS spectra of Cl 2p for Ag-Cl NP tested in 0.5 M Ar-saturated $KHCO_3$, and the carbon paper tested in the mixed solution of 0.5 M $KHCO_3$ and 0.5 M KCl.

Notes: From the spectra of Cl 2p region (blank substrate), the peaks assigned to C-Cl and Cl^- are negligible. The Cl 2p region of Ag-Cl NP tested in Ar-saturated $KHCO_3$ for 10 h only shows the existence of Cl^- ions, further indicating that above observed C-Cl bonds results from Cl^- ions and CO_2 molecular.

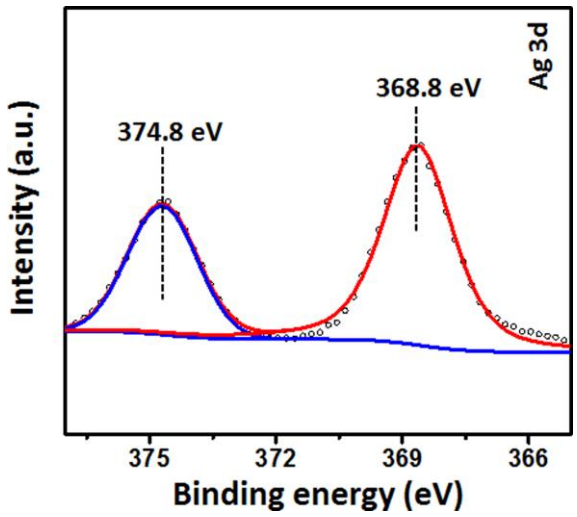

Fig. S14. The high-resolution XPS spectra of Ag 3d for Ag-Cl NP tested in 0.5 M Ar-saturated $KHCO_3$.

Notes: The Ag 3d region exhibits the same peaks position as the one tested in CO_2-saturated $KHCO_3$ (Fig. S12), demonstrating the successful reduction and existence of Ag^+.

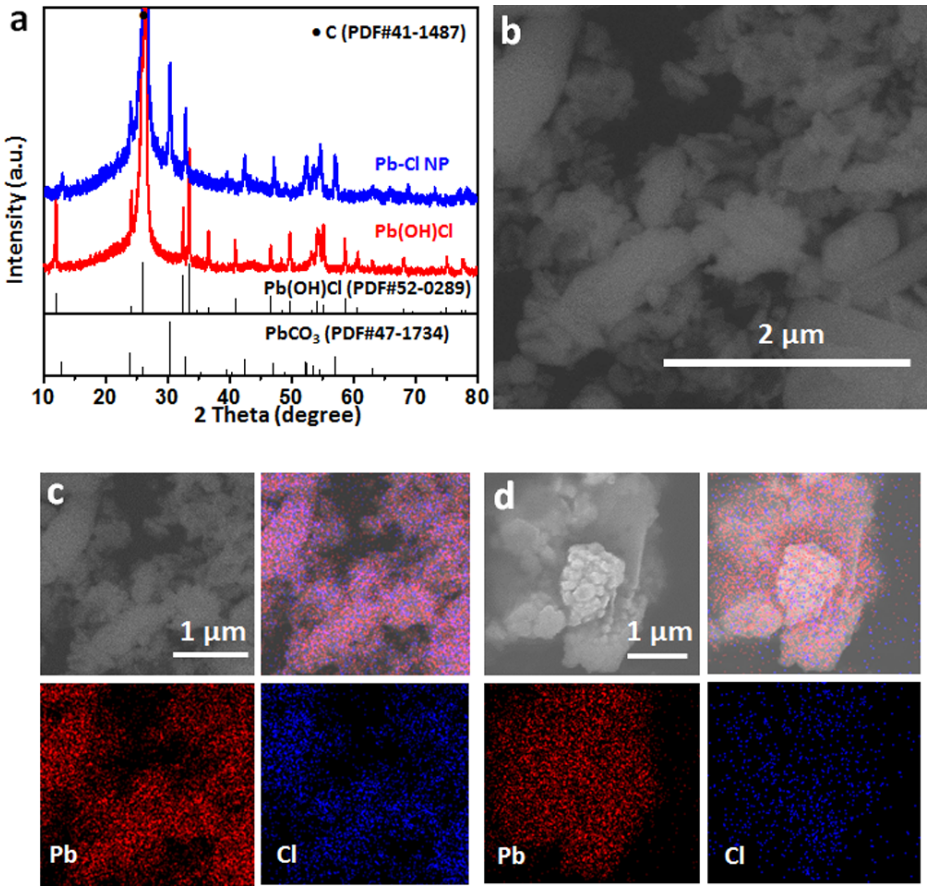

Fig. S15. (a) XRD patterns of pristine Pb(OH)Cl sample and Pb-Cl NP. (b) FESEM image of Pb(OH)Cl sample. (c) FESEM and EDX elemental mapping images of Pb and Cl for Pb(OH)Cl sample. (d) FESEM and EDX elemental mapping images of Pb and Cl for Pb-Cl NP sample.

Notes: As illustrated in Fig. S15a, the XRD pattern of the as-prepared sample shows characteristic peaks indexed to Pb(OH)Cl, and the XRD pattern of Pb-Cl NP exhibits the peaks indexed to $PbCO_3$.The elemental mapping images reveal the existence of chlorine element on both Pb(OH)Cl and Pb-Cl NP samples.

Table S1. The concentration of Cl^- ions in the electrolyte detected by the ion chromatograph analysis for pristine AgCl and Ag-Cl NP samples.

No.	Sample	Cl mg L^{-1}
1	Pristine AgCl	2.06
2	Ag-Cl NP for 5 h	39.15
3	Ag-Cl NP for 10 h	43.53

Notes: If the Cl^- anions dissolve and diffuse into the electrolyte completely, the theoretical value for concentration of Cl^- is 82.50 mg L^{-1}. The loading of AgCl is 10 mg and the solution is 30 mL 0.5 M $KHCO_3$.

Table S2. The variations of atomic percentage (At. %) for Ag and Cl elements detected by SEM energy dispersive X-ray spectroscopy (EDX) analysis with prolonging electrolysis time.

Sample	Ag (atomic pct.)	Cl (atomic pct.)
Pristine AgCl	51%	49%
Ag-Cl NP for 2000 s	89%	11%
Ag-Cl NP for 3000 s	97%	3%
Ag-Cl NP for 4000 s	98%	2%
Ag-Cl NP for 5 h	99%	1%
Ag-Cl NP for 10 h	99%	1%

Table S3. Comparison of different silver-based electrocatalysts for CO_2 electroreduction.

Catalysts	Electrolyte	Potential (V vs. RHE)	CO current density (mA cm^{-2})	FE_{CO}	Reference
Tri-Ag-NPs	0.1 M $KHCO_3$	-0.75	~ -0.60	96.8%	1
Ag nanocorals	0.1 M $KHCO_3$	-0.37	-2.00	95.0%	2
ID-Ag	0.5 M $KHCO_3$	-0.70	-16.70	94.5%	3
np-Ag	0.5 M $KHCO_3$	-0.60	-18.00	92.0%	4
OD-Ag	0.1 M $KHCO_3$	-0.80	-1.15	89.0%	5
Ag/C	0.5 M $KHCO_3$	-0.64	~ -1.50	84.4%	6
Ag/CF	0.5 M $KHCO_3$	-1.20	~ -50.00	84.0%	7
Ag-Cl NP	0.5 M $KHCO_3$	-0.80	-9.40	98.0%	This work

Notes: From the Table S3, both CO partial current density and CO Faradaic efficiency for Ag-Cl NP are comparable with other sliver-based catalysts.

Table S4. Comparison of different lead-based electrocatalysts for CO_2 electroreduction.

Catalysts	Electrolyte	Potential (V vs. RHE)	HCOOH current density (mA cm^{-2})	FE_{HCOOH}	Reference
OD-Pb	0.5 M $NaHCO_3$	-0.80	~ -0.60	98.0%	8
porous Pb	1.0 M $KHCO_3$	-0.99	-8.00	97.0%	9
Pb	0.5 M NaOH + 0.5 M NaCl	-0.96	-1.17	88.0%	10
Pb granules	0.5 M $KHCO_3$	-0.83	-0.79	90.0%	11
Pb plate	0.5 M NaOH	-0.86	-2.50	65.0%	12
Pb	0.5 M $KHCO_3$	-1.37	-31.30	43.8%	13
$Sn_{56.3}Pb_{43.7}$	0.5 M $KHCO_3$	-1.37	-45.70	79.8%	13
$Pb_{2.25}Pd_{3.75}$	0.5 M $KHCO_3$	-1.07	~-11.00	~90.0%	14
Pb/C	0.5 M $KHCO_3$	-1.33	-35.00	22.0%	15
Pb-Cl NP	0.5 M $KHCO_3$	-1.00	-10.00	92.4%	This work

Notes: From the Table S4, both HCOOH partial current density and HCOOH Faradaic efficiency for Pb-Cl NP are comparable with other lead-based catalysts.

References

1. S. Liu, H. Tao, L. Zeng, Q. Liu, Z. Xu, Q. Liu and J. L. Luo, *J. Am. Chem. Soc.*, 201**7**, **139**, 2160-2163.
2. Y. C. Hsieh, S. D. Senanayake, Y. Zhang, W. Xu and D. E. Polyansky, *ACS Catal.*, 2015, **5**, 5349-5356.
3. Y. Zhang, L. Ji, W. Qiu, X. Shi, A. M. Asiri and X. Sun, *Chem. Commun.*, 2018, **54**, 2666-2669.
4. Q. Lu, J. Rosen, Y. Zhou, G. S. Hutchings, Y. C. Kimmel, J. G. Chen and F. Jiao, *Nat. Commun.*, 2014, **5**, 3242.
5. M. Ma, B. J. Trzesniewski, J. Xie and W. A. Smith, *Angew. Chem. Int. Ed.*, 2016, **55**, 9748-9752.
6. C. Kim, H. S. Jeon, T. Eom, M. S. Jee, H. Kim, C. M. Friend, B. K. Min and Y. J. Hwang, *J. Am. Chem. Soc.*, 2015, **137**, 13844-13850.
7. S. Ma, J. Liu, K. Sasaki, S. M. Lyth and P. J. A. Kenis, *Energy Technol.*, 2017, **5**, 861-863.
8. C. H. Lee and M. W. Kanan, *ACS Catal.*, 2014, **5**, 465-469.
9. M. Fan, S. Garbarino, G. A. Botton, A. C. Tavares and D. Guay, *J. Mater. Chem. A*, 2017, **5**, 20747-20756.
10. Z. He, J. Shen, Z. Ni, J. Tang, S. Song, J. Chen and L. Zhao, *Catal. Commun.*, 2015, **72**, 38-42.
11. F. Koleli, T. Atilan, N. Palamut, A. M. Gizir, R. Aydin and C. H. Hamann, *J. Appl. Electrochem.*, 2003, **33**, 447-450.
12. B. Innocent, D. Liaigre, D. Pasquier, F. Ropital, J. M. Léger and K. B. Kokoh, *J. Appl. Electrochem.*, 2008, **39**, 227-232.
13. S. Y. Choi, S. K. Jeong, H. J. Kim, I. H. Baek and K. T. Park, *ACS Sustain Chem. Eng.*, 2016, **4**, 1311-1318.
14. X. Lu, Y. Wu, X. Yuan and H. Wang, *Angew. Chem. Int. Ed.*, 2019, **58**, 4031-4035.
15. A. Li, H. Wang, J. Han and L. Liu, *Front. Chem. Sci. Eng.*, 2012, **6**, 381-388.